08

Investigation of the magnetic-impedance properties of CuO nanoparticles obtained in a low-pressure arc discharge plasma

© A.V. Ushackov, L.Yu. Fedorov

Krasnoyarsk Scientific Center of the Siberian Branch of the Russian Academy of Sciences, Krasnoyarsk, Russia
e-mail: ushackov@mail.ru

Received May 3, 2023
Revised June 2, 2023
Accepted June 6, 2023

CuO nanoparticles obtained in a low-pressure arc discharge plasma followed by annealing in an oxygen atmosphere at 500°C were studied by X-ray diffraction and transmission electron microscopy. The formation of irregularly shaped nanoparticles in the size range of 5−30 nm was found. The Rietveld refinement confirmed the formation of a monoclinic CuO phase with an average crystallite size of ∼ 21 nm. The temperature dependences of the magnetization and permittivity of CuO nanoparticles have been studied. They show antiferromagnetic behavior with a Neel temperature of 230 K and frequency-dependent dispersion behavior in the temperature range of 100−200 K at an external magnetic field induction of 0−1.3 T. The dielectric relaxation mechanism is analyzed and found to follow the Arrhenius behavior. It is shown that hopping conductivity with a variable hop length more accurately describes charge transport in CuO nanoparticles. A magnetodielectric response of about 2.5 was observed at a frequency of 12 kHz at a temperature of 150 K in a magnetic field of 1.3 T.

Keywords: vacuum arc, oxides, nanoparticles, magnetodielectric effect.

DOI: 10.61011/TP.2023.08.57270.110-23

Introduction

Currently, the search for an effective method for the synthesis of inorganic nanoparticles with predictable morphology continues. The phase composition and size of nanoparticles play an important role in a wide range of potential applications in electronic, magnetic and photonic devices [1]. The semiconductor properties of nanostructured metal oxides and, in particular, copper oxides (particles, films, wires) find application and are promising in the manufacture of sensors, transistors, catalysis devices, photovoltaics, etc.[2–4]. Powder materials of monoclinic CuO exhibit the properties of Mott insulators, in which the electronic structure cannot be explained by classical band theory [5].

CuO nanoparticles are being actively studied for several fundamental and applied reasons: they are highly correlated electronic systems and are the basis of high-temperature cuprate-based superconductors [6,7]. The strong dependence of the semiconductor properties of CuO on the size factor and surface effects led to a revival of interest in CuO nanostructures obtained by various methods [8–10]. The size and shape of the particles can be precisely selected using a suitable synthesis method, and therefore the development of process that allows the formation of single-phase CuO nanoparticles of high purity is the most important reason for studying semiconductor, magnetic or dielectric properties. We obtained single-phase copper oxide (CuO) nanoparticles using an approach based on the evaporation-condensation method in a low-pressure arc discharge plasma [11].

The structural, optical and electronic parameters of copper oxide nanoparticles are quite well determined experimentally and are properly described in numerous papers. However, the results of the temperature dependence of the magnetization and susceptibility of CuO presented in the literature indicate unusual magnetic properties of nanoparticles [12,13]. Among all the antiferromagnetic monoxides of transition metals (CuO, MnO, CoO, NiO), copper oxide exhibits anomalous magnetic behavior, which raises interest in understanding the physics being basis of such system. As a rule, CuO exhibits non-equilibrium properties in the form of slow relaxation of magnetization and bifurcation of cooling curves FC−ZFC at low temperature. This behavior is due to the anisotropy of non-interacting nanoparticles, freezing surface spins and competitive dipole interaction in combination with randomness in the positions and orientation of the nanoparticle axes [14]. CuO exhibits magnetic order even above the Neel temperature. In addition to this, CuO exhibited a high dielectric constant (above 10^3) over a wide temperature range [15] and signs of a ferroelectrically induced magnetic transition at 230 K [16].

The purpose of this paper is to study the magnetic properties and anomalous behavior of the dielectric properties of CuO nanoparticles obtained in a low-pressure arc discharge plasma. Based on the Maxwell and Koop model, and on impedance studies data, the influence of grains and grain boundaries on the dielectric properties of CuO is considered. Besides, the influence of the magnetic field (1.3 T) on dielectric properties is considered.

1. Experiment procedure

The sample of CuO nanoparticles considered in this paper was prepared by evaporation-condensation in a low-pressure arc discharge plasma using proven technology that eliminates the formation of a microdroplet fraction [11,17]. Details of the preparation of pure single-phase CuO nanoparticles from the initially mixed $Cu/Cu_2O/CuO$ phase, of the evolution of the phase composition and calorimetry data are described in detail in previous papers [18]. To synthesize CuO nanoparticles a vacuum chamber was used with a plasma-arc evaporator mounted on the side wall, connected to welding inverter providing the arc discharge current of 100 A. A copper cylinder with a diameter of 80 mm and a purity of 99.99% was used as the evaporated cathode, and a water-cooled copper tube served as the anode. The arc discharge was ignited at a pressure of 200 Pa in a gas mixture of argon and oxygen (the ratio is 80 and 20%, respectively, in partial pressure). After condensation on cylindrical cooled surface, CuO nanoparticles in the form of a powder enter the hopper. According to X-ray diffraction studies and processing of the obtained diffraction patterns using the Rietveld method [19], the resulting powder has an average size of crystallite s of 15 nm and a mixed phase composition (5% Cu, 8% Cu_2O and 87% CuO). Next, the nanopowder was annealed at a temperature of 500°C in oxygen atmosphere for 2 h, then pressed into parallelepiped-shaped tablets of size $10 \times 5 \times 2$ mm at pressure of 10 MPa and sintered for 5 h at temperature 600°C.

Data on the phase composition of the sample were obtained using Bruker D8 Advance X-ray diffractometer with an incident radiation wavelength $CuK_\alpha = 1.5406$ Å. Transmission electron microscopy (TEM) of CuO nanoparticles was carried out on JEOL JEM-2100 high-resolution electron microscope operating at an accelerating voltage of 200 kV. The study of temperature-dependent magnetization in the range 5–350 K was carried out on vibration magnetometer based on a system for studying the physical properties of solids and nanostructures PPMS-9 (Quantum Design, USA). Studies of the temperature dependence of dielectric behavior and tangent δ of dielectric losses were performed using an impedance analyzer (FRA-24M Electrochemical Instruments, Russia) in the frequency range from 100 Hz to 100 kHz. To measure dielectric properties the contacts were made by applying silver paste to both surfaces of the sample in the form of tablets.

2. Results and discussion

The phase purity of the sample was determined using X-ray phase examination. The X-ray diffraction pattern of the CuO sample is shown in Fig. 1. The obtained data were processed using the Rietveld method using PowderCell 2.4 software. In particular, it was found that the size of the regions of coherent scattering of CuO nanoparticles is ~ 21 nm. CuO crystallizes in a monoclinic structure in

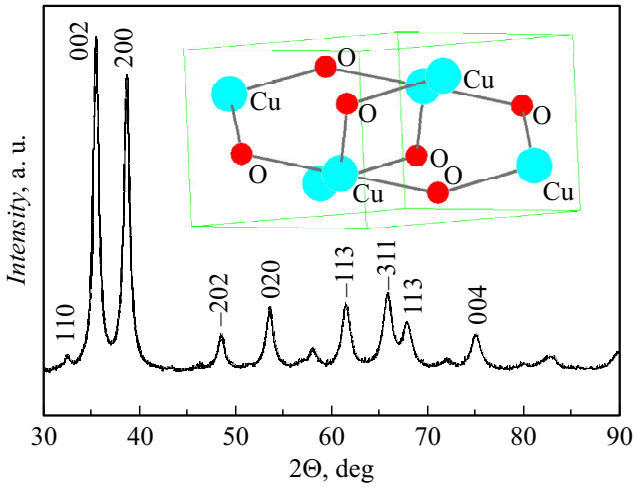

Figure 1. X-ray diffraction pattern of CuO nanoparticles (NP) formed after annealing at 500°C for 2 h in O_2 environment.

the space group C 2/c (PDF 4+ #00-045-0937). Positions of constituent atoms (x, y, z) in the crystal structure, Wyckoff positions and cell parameters (a, b and c and angleβ), as well as the fitting parameters are presented in the Table. X-ray diffraction analysis and full-profile refinement using the Rietveld method show that the crystal structure of CuO nanoparticles is single-phase, no additional impurity peaks are observed, which excludes the possibility of the secondary phases presence. The lattice parameters and unit cell volume of CuO nanoparticles were calculated and presented in the table. In the insert in Fig. 1, you can see that copper is coplanarly surrounded by four oxygen atoms, which are located at the vertices of an almost rectangular parallelogram. The sides of this parallelogram corresponding to the lengths of bonds Cu–O Cu–Cu, Cu–O, O–O, calculated as 2.900(6), 1.972(4) and 2.608(7) Å [20].

To determine the size and shape of the prepared nanoparticles, an electron microscopic study of single-phase CuO sample was carried out. A TEM image of CuO nanoparticles is shown in Fig. 2, *a*. In preliminary scanning electron microscopy images of fresh made powders the microsize fraction was absent, however, it is important to note that during the sample preparation for electron microscopy, which consists of ultrasonic dispersion of the powder removed from the substrate in isopropyl alcohol, some separation of nanoparticles by size already occurs. So, shown in Figure distribution is given for separated TEM fraction.

Irregularly shaped CuO nanoparticles in the size range 5–30 nm were observed in the photographs. Particles of the small size 5 nm, medium — 10 nm and agglomerates with a size of about 30 nm, which mainly consist of small nanoparticles, are clearly visible. The average size of particle 22 nm can be observed using the size distribution histogram shown in Fig. 2, *b*. The presence of grain boundaries is noticeable in TEM images. The thickness of the grain

Fitting parameters for modeling the diffraction pattern of CuO nanoparticles using the Rietveld method

Atom, Wyckoff position	x	y	z
Cu (4c)	1/4	1/4	0
O (4e)	0	0.43	1/4
a	4.6843(3) Å		
b	3.4230(1) Å		
c	5.1294(3) Å		
Volume	81.120 Å^3		
b	99.503(9)		
FWHM $= f(U, V, W)$	(0.5; 4.951481; −0.5)		
Preferred orientation (Rietveld model) direction (200)	o1: 5.1497 o2: 0.2344		
R_p (%)	3.82		
R_{wp} (%)	5.24		
R_{exp} (%)	2.49		

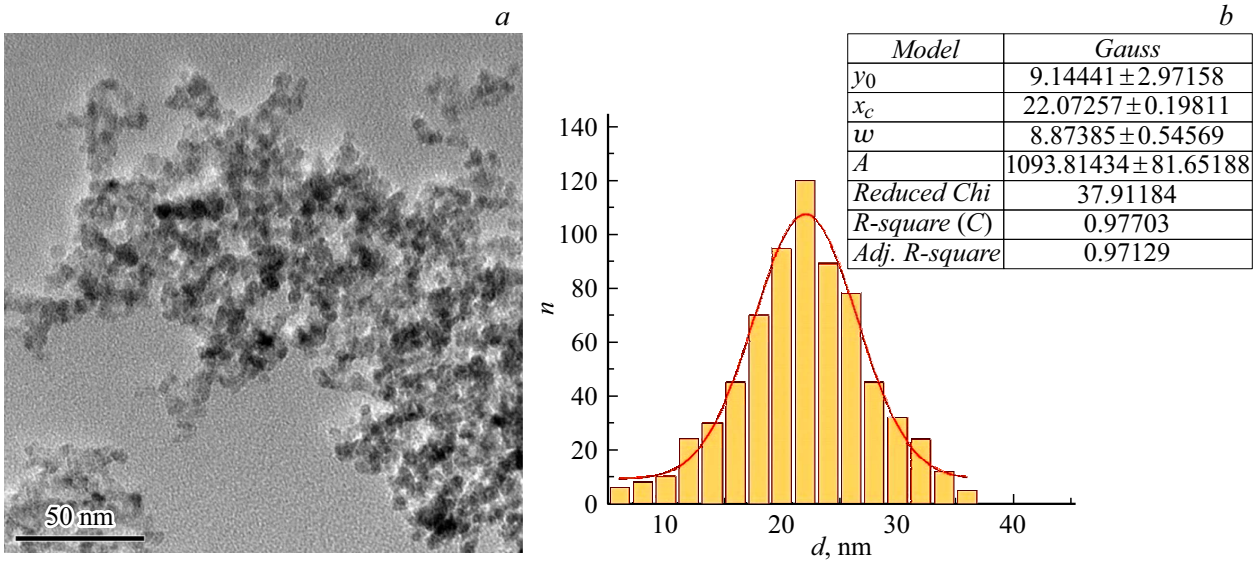

Figure 2. TEM of CuO nanoparticles (a). Size distribution of CuO nanoparticles (b).

boundaries ($\sim 2-5$ nm) can be estimated from a highly magnified image. Apparently, grain boundaries play an important role in the high values of dielectric constants observed in CuO nanoparticles.

To determine the magnetic properties, the temperature dependences of the magnetization of CuO nanoparticles in the range 5−350 K were studied. Magnetization measurements were carried out using protocols with zero field cooling (ZFC) and in field (FC) 500Òe (Fig. 3). Note that as the temperature decreases, starting from 350 K the magnetization increases slightly, and then at temperatures below ~ 230 K begins to decrease. This indicates antiferromagnetic ordering in CuO nanoparticles at this temperature, which confirms previously published data [21]. Note that the magnetization value of the prepared CuO nanoparticles was about several μemu/g.

The isothermal magnetization study carried out at various temperatures (5, 100, 200 and 300 K) and in field up to 9 T (shown in the insert in Fig. 3) was performed to better understand magnetic transition. The sample was cooled in a zero field from room temperature to a given temperature to obtain the true magnetization behavior. In the insert in Fig. 3 a nonlinearity of magnetization is observed at 5 and 100 K, which disappears on the remaining curves and, thus, confirms the antiferromagnetic behavior of CuO nanoparticles.

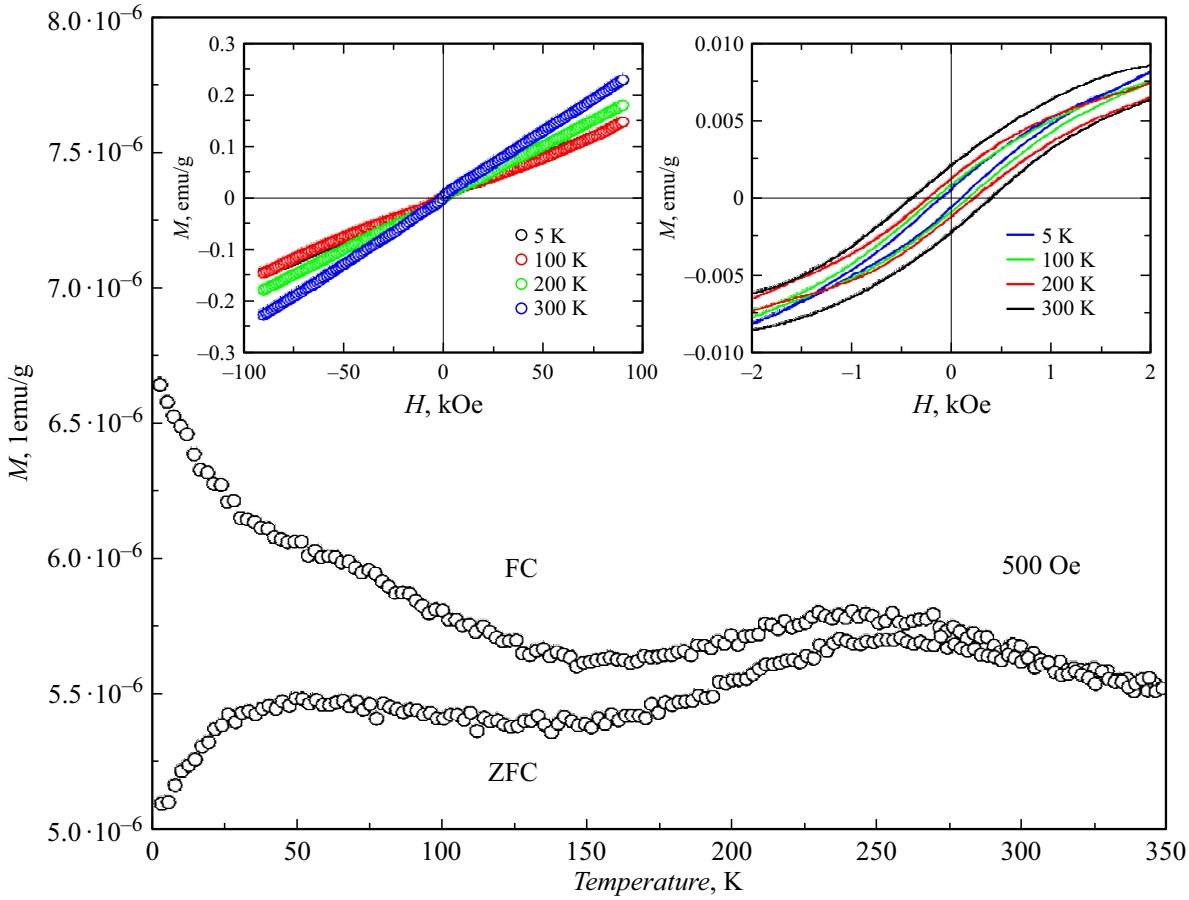

Figure 3. Magnetization vs. temperature of CuO nanoparticles in measuring field of 500 Oe. Isothermal magnetization at temperatures of 5, 100, 200 and 300 K is shown in the insert on the left, and the increased value of $M(H)$ is shown in the insert on the right.

With an increase in the magnetization curve, as shown in the left insert of Fig. 3, it becomes obvious that both ferromagnetic (FM) and antiferromagnetic (AFM) components contribute to the characteristics $M(H)$ of the resulting CuO nanoparticles at the indicated temperatures. There is a noticeable slight increase in the FM contribution associated with the prevailing AFM contribution as the temperature increases from 5 to 300 K. This behavior can also be evident from the bifurcation of the curve ZFC−FC $M(T)$.

Dielectric characteristics were measured after sample cooling to temperature ~ 10 K. Then the temperature was stabilized and the capacitance and dielectric losses were determined at fixed frequencies in the range from 500 Hz to 100 kHz in the absence of external magnetic field. The measurement was carried out up to 300 K when heated. Based on these measurements, the actual part of the dielectric constant (ε') is calculated by the formula $(Cd)/(\varepsilon_0 A)$, where C — capacitance, [F], d — tablet thickness, [m], ε_0 — absolute dielectric constant, $[8.854 \cdot 10^{-12}$ F/m], A — tablet surface area, [m^2]. Further, to study the magnetodielectric behavior of CuO nanoparticles, the measurement was repeated in the same way in the presence of external magnetic field of 1.3 T.

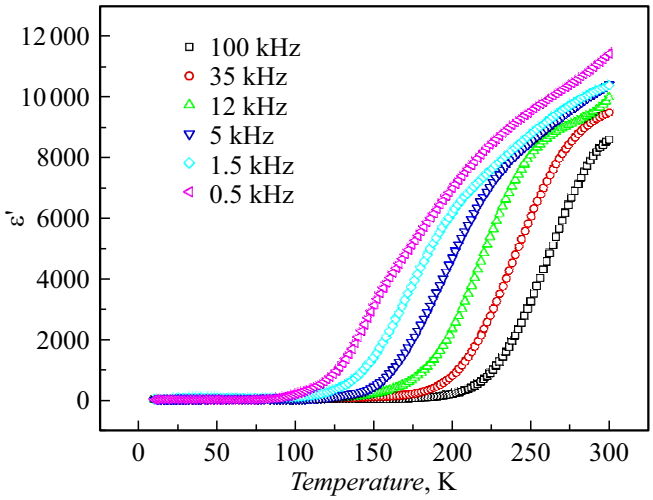

Figure 4. Dielectric constant of CuO nanoparticle vs. temperature at different frequencies.

Fig. 4 shows dielectric behavior of CuO nanoparticles vs. temperature. It can be seen that the dielectric constant (ε') remains almost constant up to 60 K, and then increases

rapidly in the temperature range 100–300 K. The increase in dielectric constant (ε') is up to three orders of magnitude. The observation of very high dielectric constant (ε') of about 10^4 at 500 Hz for CuO nanoparticles in this case corresponds to the result we obtained earlier [22]. As mentioned above, the AFM state of CuO nanoparticles is observed at 230 K. This provides „pinning“ of sublattice charge carriers, which leads to a decrease in dielectric constant. A sharp decrease at temperatures below 160 K at all measured frequencies is associated with stationary (frozen) “holes“ trapped by charge carriers in the AFM position of CuO nanoparticles. A similar high value of dielectric constant ($\varepsilon' \sim 2 \cdot 10^4$) was observed in related ceramic systems $ACu_3Ti_4O_{12}$, where A = Ca, Sr, Cd, $Bi_{2/3}$, $Ln_{2/3}$ [23,24], NiO doped by Li and Ti [25].

High value of ε' can also be caused by a thermostimulated effect. In this paper, the density of an unsintered CuO tablet was calculated, which was 6.39 g/cm^3, and after sintering the density changed slightly. The theoretical density of CuO, taking into account XRF data using the Rietveld method, was 6.41 g/cm ^{3}. From the TEM study we can also conclude that the grains are tightly packed, so the role of voids in increasing the dielectric constant is negligible.

As expected, the dielectric constant of CuO nanoparticles decreases with frequency increasing. This is due to the distortion of the dipole orientation, leading to decrease in the polarization of small crystallites. The frequency dependence of the dielectric properties of the prepared CuO nanoparticles shows dispersion.

On the other hand, on the graphs of dielectric losses vs/ temperature (tangent δ) (Fig. 5) a tendency of frequency changes can be traced. As the temperature increases, dielectric losses first increase, and after reaching the maximum value (the region containing peaks corresponding to frequencies from 500 Hz to 100 kHz, respectively, and temperatures 100–200 K) dielectric losses begin to decrease. When they reach a minimum, they begin to increase again

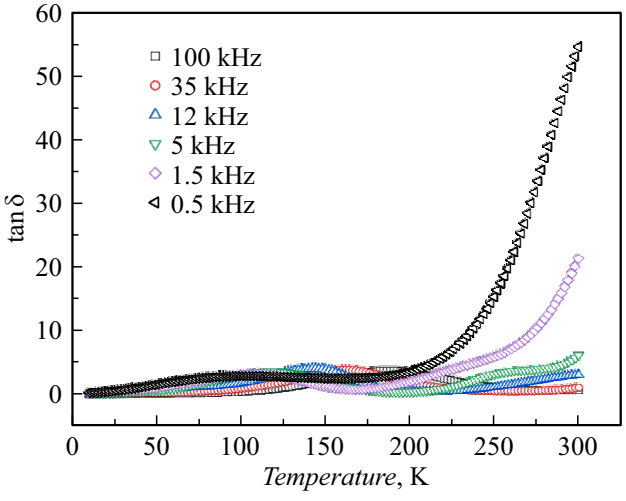

Figure 5. Dielectric loss tangent in CuO nanoparticles vs. temperature at different frequencies.

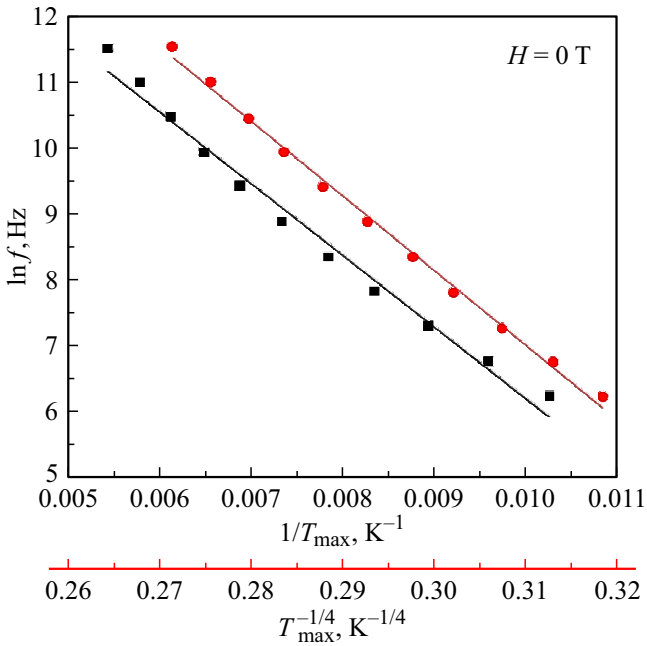

Figure 6. Logarithmic dependence of frequency (f) on $1/T_{\delta\,\max}$, displaying the temperature at the maximum dielectric loss tangent $\delta(f)$ for CuO nanoparticles. Solid lines represent the best result of approximation using the Mott model (red scale (online version)) and the Arrhenius model (black scale).

as the temperature rises. Thus, dielectric losses ($\tan\delta$) also exhibit dispersion behavior in temperature dependences. Frequency-dependent dielectric losses in CuO nanoparticles dominate in the temperature range 100–200 K with low dielectric leakage (< 5), however, ultimately, dielectric losses increase by approximately five to ten times and reach a maximum value of 60 for frequency of 500 Hz at room temperature. Taken together, based on the dependences of dielectric constant and losses, it can be concluded that CuO nanoparticles exhibit highly dispersive behavior.

To understand the relaxation dynamics of CuO nanoparticles, the temperature dependence of the maximum frequency logarithm $\tan\delta_{\max}(T)$ is approximated by the Arrhenius relation $f = f_0 \exp(-E/k_B T_{\max})$ (solid line in Fig. 6), where f_0 — pre-exponential factor, E — relaxation energy barrier, k_B — Boltzmann constant. In the region $\tan\delta_{\max}(T)$, the thermally activated relaxation reaction is described with an energy barrier E of about 0.0942 eV. However, a closer examination of the experimental results shows a deviation from the Arrhenius representation (black scale in Fig. 6). The origin of such a deviation with very low activation energy in CuO nanoparticles at a temperature around 100–200 K can be associated with the polaron relaxation mechanism [26]. The experimental result can be better approximated (red scale (in the online version) in Fig. 6) if we use the relation $f = f_0 \exp[-(T_0/T_{\max})^{1/4}]$, where f_0 and T_0 — approximation parameters [27]. This fact means that the Mott transport model of hopping-type with a variable jump length is valid only in the

low-temperature regime (< 200 K). These results can be qualitatively explained by the polaron model [28]. With this approach, a thermally activated hop with an Arrhenius dependence predominates in the high-temperature region.

Due to the aforementioned important magnetic and dielectric properties, especially the coupled behavior of FM $-$AFM and variable length hops (for $T < 200$ K) and thermally activated hops (for $T > 200$ K), an attempt was made to study the magnetic tunability of dielectric properties, i.e., the magnetodielectric effect in CuO nanoparticles.

Figure 7 shows the data on the field dependence of the dielectric constant at a fixed frequency 12 kHz. It is clear from the Figure that a moderate external magnetic field ~ 1.3 T causes a significant increase in dielectric constant (ε') in the temperature range 100$-$200 K. With a further increase in temperature, the value of the dielectric constant begins to return to behavior similar to that for zero field. To quantify the influence of the magnetic field, the insert in Fig. 7 shows the magnetodielectric coefficient as function of temperature, defined as MD $= \left([\varepsilon'(H)-\varepsilon'(0)]/\varepsilon'(0)\right)$. The dielectric constant increases by up to 2.5 times at frequency of 12 kHz at 1.3 T. At the same time MD detects a maximum at temperature ~ 140 K. This value is significantly higher at a relatively low magnetic field in a temperature range that can be easily controlled using liquid nitrogen. One of the reasons for the observed behavior of the magnetodielectric effect may be residual stresses caused by nanoscale effects, which is confirmed by the results of fitting diffraction patterns using the Rietveld method.

Additionally, in order to study the influence of the magnetic field on the dielectric characteristics, they were measured as a function of temperature at fixed frequencies under the influence of a constant magnetic field of 1.3 T. The behavior of the dielectric constant and tangent of loss angle turned out to be the same as for zero field, but the magnitude of these parameters changes. Using the tangent

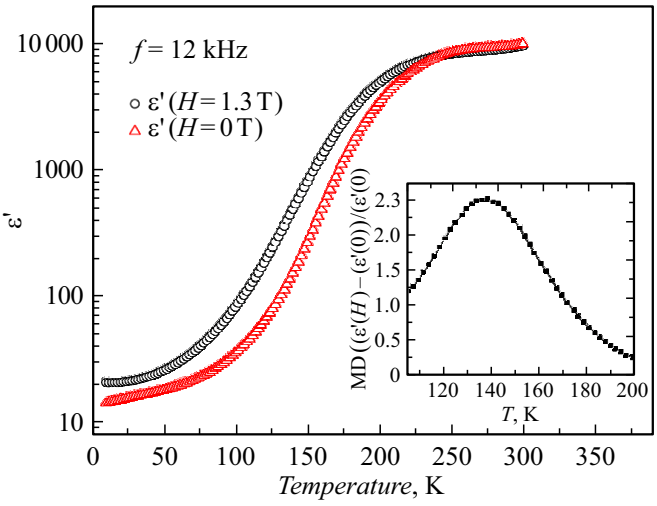

Figure 7. Temperature dependence ε', measured in applied magnetic field (1.3 T) at a fixed frequency of 12 kHz. On the insert: magnetodielectric effect in the temperature range 105$-$200 K.

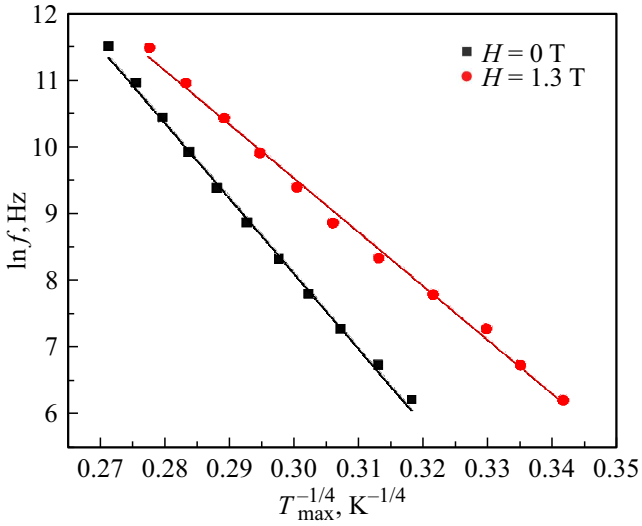

Figure 8. Logarithmic dependence of frequency (f) on $1/T_{\delta\,\max}$, displaying the temperature at the maximum dielectric loss tangent $\delta(f)$ for CuO nanoparticles in the presence of a magnetic field.

of loss angle δ, the dielectric behavior was estimated in accordance with the Mott hopping transport model with a variable hop length (Fig. 8). Data for the zero field are also given there, although with a different slope. This indicates that dielectric relaxation can be optimized by applying a magnetic field.

Conclusion

The paper investigated the structural, magnetic, dielectric and magnetodielectric properties of CuO nanoparticles obtained in low-pressure arc discharge plasma followed by oxygen annealing, pressing and sintering. Based on Rietveld's refinement, it was established that the nanoparticles were synthesized in a pure monoclinic phase of CuO with a crystallite size ~ 21 nm. Using TEM, the irregular shape of CuO nanoparticles was confirmed, the size range 5$-$30 nm with an average size ~ 22 nm. Temperature-dependent dielectric studies of CuO nanoparticles show that the dielectric relaxation mechanism in this case corresponds to the Mott hopping transport model with a variable hop length, and not to Arrhenius behavior. It is found that the magnetodielectric ratio of CuO nanoparticles reaches a peak at 140 K in a relatively low field (1.3 T). Due to the observed magnetic, dielectric, and magnetodielectric properties, CuO nanoparticles prepared using the proposed method are attractive for potential applications in devices based on fine-tuning of magnetic impedance properties.

Funding

The work has been performed under the state assignment ES-2021-0026.

Conflict of interest

The authors declare that they have no conflict of interest.

References

[1] Q. Zhang, K. Zhang, D. Xu, G. Yang, H. Huang, F. Nie, C. Liu, S. Yang. Progr. Mater. Sci., **60**, 208 (2014). DOI: 10.1016/j.pmatsci.2013.09.003

[2] S. Steinhauer. Chemosensors, **9** (3), 51 (2021). DOI: 10.3390/chemosensors9030051

[3] A. Angı, D. Sanlı, C. Erkey, Ö. Birer. Ultrasonics Sonochemistry, **21** (2), 854 (2014). DOI: 10.1016/j.ultsonch.2013.09.006

[4] A.S. Zoolfakar, R.A. Rani, A.J. Morfa, A.P. O'Mullaned, K. Kalantar-zadeh. J. Mater. Chem. C, **2**, 5247 (2014). DOI: 10.1039/C4TC00345D

[5] J.A. Spencer, A.L. Mock, A.G. Jacobs, M. Schubert, Y. Zhang, M.J. Tadjer. Appl. Phys. Rev., **9**, 011315 (2022). DOI: 10.1063/5.0078037

[6] X. Wang, L. de'Medici, A.J. Millis. Phys. Rev. B, **83**, 094501 (2011). DOI: 10.1103/PhysRevB.83.094501

[7] Yu.P. Sukhorukov, N.N. Loshkareva, A.S. Moskvin, V.L. Arbuzov, A.S. Ovchinnikov, N.M. Chebotaev, A.A. Samokhvalov. FTT, **39** (12), 2141 (1997). (in Russian).

[8] J. Leitner, D. Sedmidubský, O. Jankovský. Materials, **12** (20), 3355 (2019). DOI: 10.3390/ma12203355

[9] Y. Zhu, Z. Zhuang, Z. Liu, Z. Guo, X. Huang. J. Electroanalytical Chem., **936**, 117374 (2023). DOI: 10.1016/j.jelechem.2023.117374

[10] I.V. Karpov, A.V. Ushakov, V.G. Demin, E.A. Goncharova, A.A. Shaihadinov. JOM, **72**, 3952 (2020). DOI: 10.1007/s11837-020-04221-5

[11] A.V. Ushakov, I.V. Karpov, L.Yu. Fedorov, E.A. Goncharova, M.V. Brungardt, V.G. Demin. Tech. Phys., **67** (15), 2410 (2021). DOI: 10.21883/TP.2022.15.55268.157-21

[12] E. Batsaikhan, C.-H. Lee, H. Hsu, C.-M. Wu, J.-C. Peng, M.-H. Ma, S. Deleg, W.-H. Li. ACS Omega, **5** (8), 3849 (2020). DOI: 10.1021/acsomega.9b02913

[13] A.A. Samokhvalov, T.I. Arbuzova, V.V. Osipov, N.A. Viglin, S.V. Naumov, N.I. Solin, B.A. Gizhevsky, I.B. Smolyak, V.A. Teplov, V.P. Pilyugin. FTT, **38** (11), 3277 (1996). (in Russian).

[14] A.V. Ushakov, I.V. Karpov, A.A. Lepeshev, M.I. Petrov, L.Yu. Fedorov. Phys. Solid State, **57** (5), 919 (2015). DOI: 10.1134/S1063783415050303

[15] H.C.R. Bitra, A.V. Rao, K.S. Babu, G.N. Rao. Mater. Chem. Phys., **254**, 123379 (2020). DOI: 10.1016/j.matchemphys.2020.123379

[16] Z. Wang, N. Qureshi, S. Yasin, A. Mukhin, E. Ressouche, S. Zherlitsyn, Y. Skourski, J. Geshev, V. Ivanov, M. Gospodinov, V. Skumryev. Nature Commun., **7**, 10295 (2016). DOI: 10.1038/ncomms10295

[17] A.V. Ushakov, I.V. Karpov, A.A. Lepeshev, M.I. Petrov. Vacuum, **133**, 25 (2016). DOI: 10.1016/j.vacuum.2016.08.007

[18] L.Yu. Fedorov, I.V. Karpov, A.V. Ushakov, A.A. Lepeshev. Inorgan. Mater.: Appl. Res., **9** (2), 323 (2018). DOI: 10.1134/S2075113318020107

[19] H.M. Rietveld. J. Appl. Cryst., **2**, 65 (1969).

[20] G. Döring, C. Sternemann, A. Kaprolat, A. Mattila, K. Hämäläinen, W. Schülke. Phys. Rev. B, **70**, 085115 (2004). DOI: 10.1103/PhysRevB.70.085115

[21] T.I. Arbuzova, S.V. Naumov, V.L. Arbuzov, K.V. Shalnov, A.E. Ermakov, A.A. Mysik. FTT, **45** (2), 290 (2003). (in Russian).

[22] A.A. Lepeshev, N.A. Drokin, A.V. Ushakov, I.V. Karpov, L.Yu. Fedorov, E.P. Bachurina. J. Mater. Sci.: Mater. Electron., **29** (14), 12118 (2018). DOI: 10.1007/s10854-018-9319-2

[23] O.Z. Yanchevskii, O.I. V'yunov, A.G. Belous, L.L. Kovalenko. J. Alloys Compounds, **874**, 159861 (2021). DOI: 10.1016/j.jallcom.2021.159861

[24] M.M. Ahmad, A. Alshoaibi, S.A. Ansari, T.S. Kayed, H.A. Khater, H.M. Kotb. Materials, **15** (9), 3173 (2022). DOI: 10.3390/ma15093173

[25] J. Wu, C.-W. Nan, Y. Lin, Y. Deng. Phys. Rev. Lett., **89** (21), 217601 (2002). DOI: 10.1103/PhysRevLett.89.217601

[26] L. Zhang, Z.-J. Tang. Phys. Rev. B, **70**, 174306 (2004). DOI: 10.1103/PhysRevB.70.174306

[27] N.F. Mott, E.A. Davis. *Electronic Processes in Non-Crystalline Materials* (Clarendon Press, Oxford, 1979)

[28] S. Mukherjee, S. Chatterjee, S. Rayaprol, S.D. Kaushik, S. Bhattacharya, P.K. Jana. J. Appl. Phys., **119**, 134103 (2016). DOI: 10.1063/1.4945318

Translated by I.Mazurov